Journal of Materials Chemistry C

ROYAL SOCIETY OF CHEMISTRY

PAPER

View Article Online
View Journal

Cite this: DOI: 10.1039/d6tc00536e

Energy dissipation and electromechanical response in dielectric actuation of liquid crystal elastomers

Justin M. Speregen,[a] Abigail Hurd,[b] Hayden E. Fowler [b] and Timothy J. White *[ab]

Dielectric liquid crystal elastomer actuators (DLCEAs) offer a promising route to low-density actuators with directional control and high power density. Improving the strain response of DLCEAs relative to traditional dielectric elastomer actuators (DEAs) remains an important step toward their use in functional applications such as robotics. Classical DEA theory predicts that strain should scale with the dielectric constant of the active material. Guided by this framework, we prepared and investigated a series of monodomain aligned liquid crystal elastomers (LCEs based on a common liquid crystalline monomer copolymerized with a range of high-dielectric comonomers. These compositional modifications increased the dielectric constant by more than fifty percent; however, DLCEA actuation did not yield the expected increase in strain. To understand this discrepancy, we performed extensive mechanical and dielectric characterization to identify factors suppressing the electromechanical response. Despite increases in dielectric constant, overlap of the mechanical loss peak with the actuation temperature emerges as a dominant dissipation pathway that limits electromechanical transduction. In addition, dielectric losses associated with conductive mechanisms further suppress actuation. Consistent with these findings, DLCEAs combining high dielectric constant with high mechanical loss require extended time scales to approach equilibrium strain. Compared to conventional DEA materials, LCEs exhibit both larger magnitudes and distinct modes of dissipation, which can amplify the role of loss in limiting DLCEA electromechanical performance.

Received 19th February 2026,
Accepted 1st May 2026

DOI: 10.1039/d6tc00536e

rsc.li/materials-c

Introduction

Liquid crystal elastomers (LCEs) are promising "low density actuators" as stimuli-responsive polymeric materials.[1–4] LCEs are loosely crosslinked networks that incorporate liquid crystalline monomers composed of rod-like mesogens whose intermolecular interactions promote orientational order.[5,6] Because the liquid crystalline phase can be retained after polymerization, macroscopic shape change can be realized by heating the material through the liquid crystalline order–disorder transition.[7–9] Spatial variation of mesogen orientation enables a wide range of programmed deformation modes including bending, twisting, and combinations thereof, such as cone formation.[10–13] The distinctive stimuli-response of LCE has motivated extensive investigation of LCEs as artificial muscles and soft robotic actuators. Although the shape programmability and specific work output of thermotropically actuated LCEs are compelling, the response time, energy efficiency, and requirements for thermal cycling limit their applicability. Thermotropic actuation frequencies exceeding one hertz are generally restricted to micro/nanoscale actuators.[14,15] Even with rapid and efficient heat transfer/exchange approaches, the time-dependent process of mesogen reorientation fundamentally limits actuation speed and efficiency.

Dielectric elastomer actuators (DEAs) are a class of electrically stimulated actuators that have shown promise due to their high energy efficiencies and cycle frequencies.[16–21] This results in power-to-weight ratios that can exceed human muscle.[22–28] A DEA device consists of an insulating elastomer, polarizable by an external electric field, that is coated on both sides with compliant electrodes.[29] This enables the application of a through-thickness electric field across the elastomer, and the resultant compressive/equibiaxial Maxwell stresses can quickly induce in-plane expansion concurrent to thickness compression. The original report from Kornbluh and Pelrine proposed a small strain approximation[17] to simplify the mechanics of DEAs to the relationship presented in eqn (1), relating the

[a] Materials Science and Engineering Program, University of Colorado Boulder, Boulder, CO, 80309, USA. E-mail: tim.white@colorado.edu
[b] Department of Chemical and Biological Engineering, University of Colorado Boulder, Boulder, CO, 80309, USA

electromechanical response (strain) to the strength of the applied electric field (V) and material properties and geometry where ε' is the real relative permittivity, z is the elastomer thickness/length of the electric field, and Y is the modulus.

$$\text{Strain} = \frac{\varepsilon' V^2}{Y z^2} \quad (1)$$

Realizing directional actuation (areal or volumetric) in DEAs prepared from conventional polymeric materials with isotropic moduli is not possible without external constraints. The simplest and most common method used to introduce anisotropy in the electromechanical response is through mechanical biasing such as asymmetric prestretch. Many DEA devices are based on commercially available elastomers, including acrylics such as VHB (3M)[30,31] and silicones such as Sylgard (Dow Chemical),[32–35] although a wide range of alternative polymeric formulations have been explored.[36–39] The primary advantage of this approach is the use of materials that are readily available and, in some cases, serendipitously optimized for DEA performance, including exceptionally low elastic moduli, unusually high dielectric constants, or reduced ionic conductivity through suppression of mobile impurities. The principal limitation, however, is that achieving directional displacement in these systems requires rigid frames or external mechanical constraints, which complicate integration, reduce conformability, and increase device density without contributing to actuation efficiency or effectiveness.[40,41] Accordingly, DEAs prepared from intrinsically mechanically anisotropic materials such as liquid crystal elastomers (LCEs) offer immediate advantages in reducing device density, improving conformability, and enabling efficient electromechanical coupling without external constraints.[42,43] Several recent reports have described the initial demonstration and subsequent development of dielectric liquid crystal elastomer actuators (DLCEAs).[44–48] Notably, the intrinsic programmability of LCEs allows monolithic polymeric materials to be encoded with spatial variations in mechanical properties, enabling distinctive areal and volumetric deformation modes under electrical stimulation.

In a prior study, we reported the synthesis, alignment, and electromechanical characterization of an aligned dielectric liquid crystal elastomer actuator (DLCEA) that achieved uniaxial strains approaching 17.5 percent.[47] This relatively high strain was attributed to the combination of a soft elastomeric network with strong modulus anisotropy arising from liquid crystal alignment. In accordance with the approximation originally described by Kornbluh and Pelrine, the electromechanical strain in a dielectric elastomer actuator is expected to scale with the ratio of dielectric constant to elastic modulus under an applied electric field. Within this framework, the observed strain response of the initial DLCEA formulation appeared broadly consistent with Maxwell-stress-based predictions, motivating further exploration of compositional strategies to enhance dielectric response while maintaining favourable mechanical properties.

Guided by this relationship, we investigated a series of aligned LCE compositions designed to increase relative permittivity while approximately preserving elastic compliance. This was accomplished by substituting the non-mesogenic dithiol comonomer used previously with alternative thiol comonomers bearing permanent dipoles or more polarizable chemical linkages. While this approach successfully increased dielectric constant, and in some cases reduced elastic modulus perpendicular to the alignment direction, compositional changes inevitably altered both dielectric and mechanical properties. Notably, increases in the $\varepsilon'/Y_\perp$ quotient did not translate into systematic improvements in actuation strain, indicating that dielectric constant and modulus alone are insufficient predictors of DLCEA performance. These observations suggest that additional factors, absent from the idealized model, play a critical role in governing the electromechanical response of DLCEAs.

In contrast to conventional dielectric elastomer actuators, where viscoelastic and dielectric losses are often mitigated through prestretch,[49–51] material selection, and device architecture, DLCEAs rely on intrinsically anisotropic, softly crosslinked polymer networks that frequently operate near their glass transition temperature. As a result, both mechanical dissipation and electrical loss mechanisms are expected to be more prominent. While loss processes in silicone- and acrylate-based DEAs have been extensively studied[52–56] and are typically secondary to actuation performance, comparable systematic investigations have not been carried out for DLCEAs. This gap is particularly important given that DLCEAs aim to achieve directional actuation through material-level programmability rather than external constraints. Accordingly, the present work focuses on disentangling the roles of mechanical and dielectric dissipation in DLCEAs, providing a framework for understanding when and why the idealized approximations break down in these systems.

Experimental

Alignment cell preparation

Glass slides were plasma cleaned for 10 minutes and then spin coated with 0.125 wt% Elvamide (Dupont) dissolved in MeOH at 3500 rpm for 1 minute. Elvamide coated slides were rubbed in the desired alignment direction with a felt cloth for 1 minute. Two rubbed slides were glued together with antiparallel rubbing using Norland 68 optical adhesive mixed with 15 or 30 μm silica bead spacer. The optical adhesive was cured *via* 3 minutes of UV light exposure.

LCE synthesis and alignment

LCEs were prepared from liquid crystalline monomer, 1,4-bis-[4-(6-acryloyloxy-hexyloxy)benzoyloxy]-2-methylbenzene (C6M, Wilshire Technologies), photoinitiator, 2-Benzyl-2-dimethylamino-1-(4-morpholinophenyl)-butanone-1 (I-369, iGM Resins), inhibitor, 4-methoxyphenol (MEHQ, Sigma-Aldrich), and the following thiol-functionalized comonomers: 1,6-hexanedithiol (HDT, Sigma-Aldrich), 1,4-benzenedimethanethiol (BDMT, Sigma-Aldrich), benzyl mercaptan (BM, Sigma-Aldrich), 4-(mercaptomethyl)benzonitrile (CN-BM, Sigma-Aldrich), 4-bromobenzyl

mercaptan (Br-BM, Sigma-Aldrich), and 2,2′-(ethylenedioxy)-diethanethiol (EDDET, Sigma-Aldrich). All LCE compositions were composed of 65 mg of liquid crystal monomer (C6M) combined with an equimolar amount of a single thiol-functionalized non-liquid crystalline comonomer (HDT, BDMT, BM, CN-BM, Br-BM, or EDDET) along with 1.5 wt% I-369, and 0.5 wt% MEHQ. All solid components were melt mixed at 150 °C *via* alternation between heat gun and vortex mixer. The mixture was placed on a hot plate at 90 °C (above the order–disorder transition temperature). If applicable, the liquid component (HDT, BM, or EDDET) was added and melt mixed *via* alternation between hot plate and vortex mixer. The mixture was capillary filled into a single 30 μm or two 15 μm alignment cells at 90 °C. Once full, alignment cells were annealed at 45 °C (below the order–disorder transition temperature) for a minimum of two minutes until birefringence was visually observed by rotating the cell between cross polarizers. Filled and annealed alignment cells were photopolymerized using 365 nm light at 150 mW cm^{-2} for 10 minutes unless otherwise noted. Aligned LCE was harvested by soaking the alignment cell in water and carefully prying a razor blade into a glued corner. With the razor inserted, the cell is placed back into water to allow the cell to open without cracking the glass or tearing the aligned LCE.

Mechanical characterization

All mechanical testing was conducted with TA Instruments Dynamic Mechanical Analyzer 850 equipped with a liquid nitrogen cooling system controlled by TA Instruments TRIOS software. All mechanical testing was under uniaxial tensile conditions. 30 μm thick aligned LCE strips were cut (~3 mm wide, ~12 mm long) *via* razor blade either perpendicular or parallel to the alignment director. Opposite ends of LCE were secured to tensile clamps *via* Kapton tape. Prior to any mechanical testing, the DMA850 applied a 5 mN preload to ensure samples were in tension. This uniaxial preload is roughly equivalent to the preload utilized for actuation testing.

Tensile testing was taken until failure at ambient conditions at a constant strain rate of 10%/min. Young's modulus was calculated by performing a linear fit of the linear low strain (<3%) regime. Frequency-dependent dynamic mechanical analysis was performed under ambient conditions at a 0.5% strain amplitude from 0.1 Hz to 10 Hz (ten points per decade). Temperature-dependent dynamic mechanical analysis was performed from −20 °C to 50 °C at a heating rate of 2 °C min^{-1}, a 0.5% strain amplitude, and frequency of 1.0 Hz.

Dielectric characterization

LCE dielectric properties were assessed in standard two-electrode setup *via* potentiostatic electrochemical impedance spectroscopy with a Gamry Reference 620 potentiostat controlled by Gamry Frameworks software. Electrodes were prepared by painting aqueous dispersion of single-walled carbon nanotubes onto PTFE tape-masked 30 μm aligned LCE film. After drying, coating was repeated on the same surface area on the other side of the film following the same procedure. Copper tape was attached to both electrodes as leads. The device is sandwiched between VHB 4910 tape to improve lead contact with electrode and reduce measurement noise. DS was performed at V_{rms} = 1.0 V over the frequency range of 10^{-1} to 10^{6} Hz. The recorded spectra was converted into real and imaginary capacitance values over the entirety of the frequency range using Gamry Echem Analyst Software. Eqn (2) and (3) were used to extract real and imaginary relative permittivity from capacitance values/sample dimensions, and eqn (4) calculates the dielectric loss tangent:

$$\varepsilon' = \frac{C_r z}{\varepsilon_{0A}} \tag{2}$$

$$\varepsilon'' = \frac{C_i z}{\varepsilon_{0A}} \tag{3}$$

$$\tan(\delta)_{dielectric} = \frac{\varepsilon''}{\varepsilon'} \tag{4}$$

ε' and ε'' are the real relative permittivity (dielectric constant) and imaginary relative permittivity respectively, C_r and C_i are the real and imaginary capacitance respectively in F, z is the LCE thickness in m, A is the electrode area in m^2, ε_0 is the permittivity of free space (8.85×10^{-12} F m^{-1}), and $\tan(\delta)_{dielectric}$ is the dielectric loss tangent.

Actuator fabrication and characterization

Two 15 μm aligned LCEs prepared from the same prepolymer mixture were laminated together while on their original glass substrate at 65 °C under manually applied compressive pressure. Samples were masked on both sides with PTFE tape and then clamped on opposite sides by in-house laser-cut acrylic frames. Electrodes were prepared by carefully applying carbon grease to unmasked regions of LCE on both sides. The mask was removed and copper tape was attached to both electrodes to act as leads. Electrodes had a minimum gap of 5 mm from the sample edge to prevent electric field arcing between them.

The top acrylic frame is used to hang the LCE vertically, and the bottom acrylic frame (mass = 5 g) acts as a small preload to keep the sample in tension prior to biasing. The LCE was orientated such that the alignment director was horizontal, so deformation was predominantly vertical. Voltage between electrodes was controlled during actuation *via* Trek 610E high voltage source. A 100 V potential was applied prior to any testing to ensure no shorting. Strain-voltage data was gather by applying a DC bias in 500 volt intervals for approximately 5 seconds. Maximum strain at a given voltage is reported herein. LCEs were allowed to fully recover between each potential tested. Actuation was video recorded and used to normalize electrode deformation by original electrode height to yield the actuation strain. Length/strain measurements of videos were assisted by Tracker Video Analysis and Modeling Tool and ImageJ software. For calculating the applied electric field, the distance over which the voltage is applied was approximated by the original sample thickness (30 μm).

Long-time DC actuation testing/fitting

DLCEAs were prepared as previously described. DC voltage of 2.5 kV was applied to 30 μm thick actuators until dielectric breakdown. Viscoelastic actuation and relaxation processes fit well to stretched exponential. Actuation and relaxation curves were fit to eqn (5) in OriginLab where the fit's parameters were the strain at infinite time (ε_∞), the time constant (τ) and the stretching factor (α). The only constraint was the strain parameter could not be negative as there is was no compressive stress along the measured axis.

$$\varepsilon(t) = \varepsilon_\infty + (\varepsilon_0 - \varepsilon_\infty) \times \exp\left(-\frac{t}{\tau}\right)^{\alpha}. \quad (5)$$

Other material characterization

Gel fractions of LCE were measured by soaking aliquots of aligned and cured LCE film in dichloromethane for 24 h and then allowing to completely dry. The mass of the dried LCE divided by its mass prior to soaking in solvent is noted as the gel fraction.

The prepolymer mixture for real-time infrared spectroscopy (RTIR) is prepared as previously outlined. The pre-polymer mixture is placed in between two salt plates. The absorption of the acrylate ($\sim 810\ cm^{-1}$) and thiol ($\sim 2550\ cm^{-1}$) peaks were monitored over 10 minutes following UV light exposure. Conversion was reported by comparing the areas under each peak at each time compared to the initial area under the peak.

Glass transition temperatures of LCEs were measured *via* differential scanning calorimetry (DSC) using a TA Instruments Discovery DSC 2500. Samples of approximately of 5 mg underwent a heat-cool-heat cycle ranging from −40 to 180 °C at a constant heating/cooling rate of 5 °C min^{-1}. The onset of the second order transition on the second heat ramp is reported as the glass transition temperature from DSC.

Results and discussion

In 2021, an initial study of LCE-HDT polymerized an equimolar amount of liquid crystal monomer (C6M) and 1,6-hexanedithiol (HDT) comonomer.[47] Herein, a series of derivative LCEs were synthesized through one-pot thiol-acrylate photopolymerization adhering to previously reported method. Each prepolymer mixture contains a 1 : 1 molar ratio between liquid crystalline diacrylate monomer, C6M, and a single non-liquid crystalline thiol-functionalized comonomer from the series of structures shown in Fig. 1a. This series of comonomers feature permanent dipoles to bolster dielectric constant. Differences between comonomers' substituent bulk and polarizability enable simultaneous analysis of resultant permittivity, dielectric strength, and viscoelastic mechanics.

Upon coating LCEs on both sides with compliant electrode, an applied through-thickness voltage results in the accumulation of charge at the electrode-LCE interfaces. Coulombic forces generate a compressive/equibiaxial Maxwell stress and a resultant shape change. For an unbiased isotropic dielectric elastomer, these Maxwell stresses promote uniform planar expansion synchronous with thickness reduction. LCEs are intrinsically anisotropic, featuring a distinctly lower Young's modulus and higher strain to failure, perpendicular to the nematic director. Prior to curing, the LCE melt is cooled to the nematic phase such that mesogens are locally orientationally ordered. Alignment layers at both of the LCE surfaces promote a monodomain nematic phase *i.e.* mesogen direction is globally correlated.[57,58] Using these monodomain nematic LCEs as the active layer in a DEA device converts the equibiaxial Maxwell stress to uniaxial deformation (Fig. 1b). More complex director profiles can be programmed to realize more complicated actuation modalities, but the uniaxial strain response of monodomain nematic LCEs enables more facile analysis of the underlying composition-property relationships governing DCLEA performance.

Mechanical behavior of all LCEs is characterized by uniaxial tensile testing parallel and perpendicular to the nematic director (Fig. 1c). High contrast between these moduli ensures the majority of planar expansion is uniaxial during compressive loading.[43] Deformation perpendicular to the director occurs in three distinct regimes: an initial linear-elastic regime, a soft elastic plateau at intermediate strains, and then strain hardening prior to failure. The slope of the linear elastic regime, Young's modulus, succinctly characterizes the stress–strain relation from approximately 0% to 20% strain in a single parameter. The soft elastic plateau is a feature unique to LCEs deformed nonparallel to the director. Strain reversibly increases under minimal stress conditions due to mesogen reorientation to the loading direction.[59] The magnitude and length of this plateau is highly formulation and alignment dependent. This viscous nature of this process introduces stress/strain rate dependence. These mechanically driven mesogen reorientation processes, in addition to the intrinsic anisotropy of LCEs, differentiate DLCEA behavior from that of traditional elastomers. The mechanical loss factor, tan(δ), and the storage modulus (cyclic analog to Young's modulus) were measured in tensile loading over a range of temperatures at 1 Hz for all LCEs (Fig. 1d). In this context, tan(δ) is a measure of the energy lost to dissipative mechanical processes per cycle. LCEs all undergo a thermomechanical transition from the glassy to rubbery state at the glass transition temperature (T_g). At T_g, tan(δ) exhibits a broad peak accompanied by a drop in storage modulus by orders of magnitudes.

The real and imaginary components of permittivity were measured over seven decades of frequencies by dielectric spectroscopy (DS) (Fig. 1e). The real permittivity/dielectric constant of the LCE (ε') quantifies the material's ability to store charge under an applied electric field, while the imaginary permittivity (ε'') captures energy lost from polarization or conduction. $\varepsilon''/\varepsilon'$ defines the dielectric loss factor, tan(δ), a measure of energy lost per cycle to dissipative electronic processes. At $\sim 10^5$ Hz, there is a resonance peak in ε'' concurrent with a sharp decrease in ε', marking the cut-off frequency for dipole response time.[60,61] Below the cutoff frequency, the electric field varies on timescales commensurate with molecular relaxation, allowing dipoles to respond quasi-statically. The mechanical response time of DLCEAs confines actuation to low frequencies

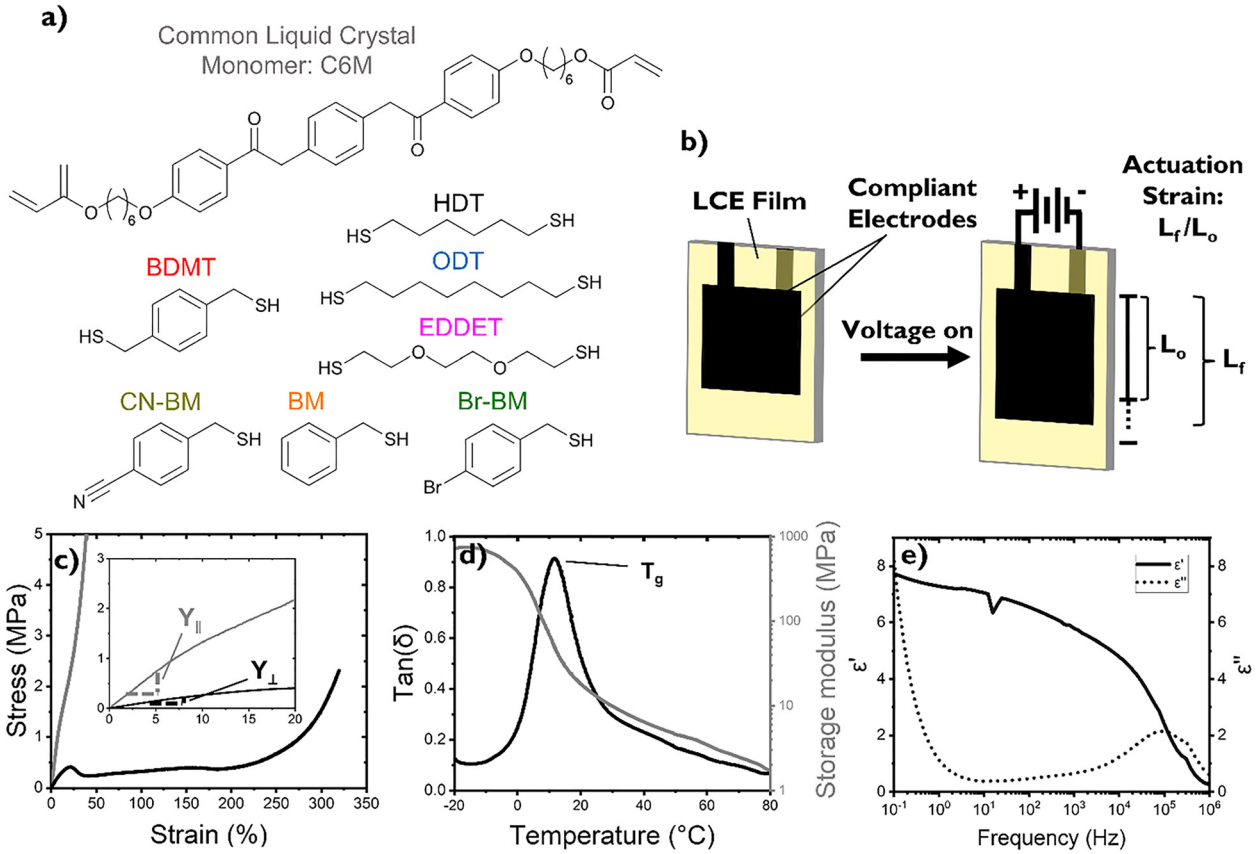

Fig. 1 (a) Chemical structures of liquid crystalline monomer and thiol comonomers. (b) Schematic of DLCEA electromechanical actuation. The intrinsic anisotropy of LCE does not require mechanical bias. Accordingly, application of a field to compliant electrodes can result in an directional deformation on the soft modulus axis of the material (orthogonal to the nematic director). Relevant material properties of LCE (LCE-HDT) is presented in (c) tensile deformation parallel and perpendicular to the director, (d) dynamic mechanical analysis perpendicular to the director, and (e) real and imaginary relative permittivity from dielectric spectroscopy.

($\lesssim 10^3$ Hz), where dipole reorientation dominates dielectric response.[47] Introducing stronger dipoles or flexible chains that readily reorient under field increases ε' in this regime. The low-frequency tail ($\lesssim 1$ Hz) of imaginary permittivity is due to ionic conduction. This is corroborated by the characteristic $\varepsilon'' \propto \omega^{-1}$ behavior in the imaginary electric modulus below the conductivity-relaxation peak (Fig. S1e and f). Although ion poling inflates ε', the associated ionic conductivity is detrimental to DLCEA actuation. A shift of ionic conduction to higher frequencies correlates with faster dielectric failure and reduced breakdown voltage.

According to accepted DEA theory, the compressive Maxwell stress equals the product of squared electric field and the absolute real permittivity of the elastomer (eqn (1)).[17] Consequently, DEA strain response is directly proportional to the real dielectric constant of the elastomer and quadratically proportional to the applied electric field. At a critical threshold voltage, the active layer allows charge flow through the bulk. This DEA failure mode, dielectric breakdown, forms a conducting pathway between electrodes, thereby rendering the device inoperable. Thus, the maximum applicable Maxwell stress increases quadratically with breakdown voltage. The mechanical stiffness of an LCE, characterized *via* tensile modulus, governs the magnitude of strain at a given applied stress. This classical description of DEAs assumes ideal behavior: mechanical deformation is modeled hyperelastically and charge storage is modeled as a lossless ideal capacitor. In the aggregate, these fundamental relations underscore the key intrinsic material properties for DEA materials, namely, high breakdown voltage and dielectric constant coupled with low modulus.

Dielectric spectroscopy, summarized in Fig. 2, confirms that the non-mesogenic comonomer has a profound effect on the dielectric constant. Hebner *et al.* report that when BDMT is copolymerized with C6M, on average each dithiol monomer singly reacts, forming one sulfide group and a dangling thiol.[62] Therefore, the pendant thiol can be substituted with an alternative functionality without inhibiting photopolymerization. All thiol comonomers reached ~50% thiol conversion by RTIR, and gel fractions exceeded 95%, confirming effective incorporation into the polymer network (Fig. S3). Fig. 2a contrasts the dielectric constant for each comonomer. At the highest frequency measured, 10^6 Hz, differences are negligible, as the field switches too rapidly for dipolar reorientation to contribute. Fig. 2b compares the cutoff frequency of dipolar reorientation; at frequencies lower than the ε'' peak, contributions from dipoles substantially raise the dielectric constant. Across

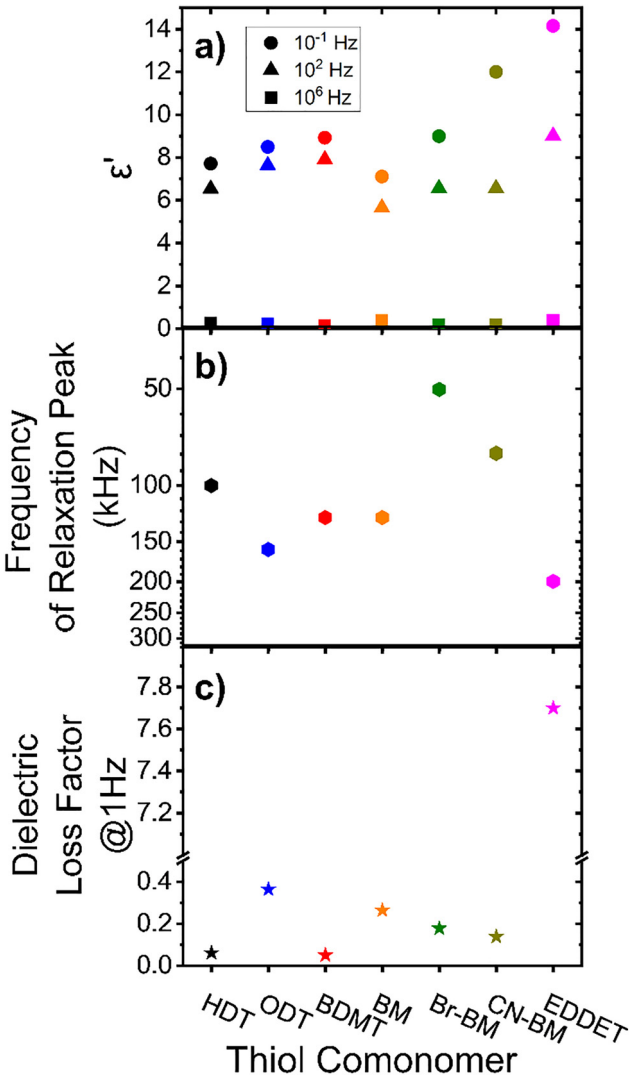

Fig. 2 (a) Dielectric constant of LCEs at various frequencies. This determines the magnitude of applied Maxwell stress at a given frequency in DEA configuration. (b) Frequency of relaxation peak, above which, permanent dipoles can no longer contribute to the dielectric constant (c) Dielectric loss factor for all LCEs at 1 Hz, reflecting differences in low frequency ion conduction.

all LCEs tested, this crossover frequency is well above the mechanical response time of DLCEAs. Fig. 2c compares the low-frequency loss factor ($\varepsilon''/\varepsilon'$). A combination of polarization and conduction losses contribute to dielectric loss. Higher energy loss per cycle causes quicker/lower-voltage dielectric breakdown.

LCE-BM is comparatively stiff and has the least amount of permanent dipoles resulting in the lowest ε' measured. The increase in ε' of LCE-BDMT relative to LCE-BM suggests that the relatively weak thiol dipole increases bulk permittivity. In the regime relevant to actuation ($\lesssim 10^2$ Hz), ε' of all dithiols (HDT, ODT, and BDMT) and Br-BM are similar. Despite the high polarity of the C–Br bond, the low dielectric constant and low frequency of the relaxation peak suggests poor reorientation under field.

Nitrile functionalities have been utilized to engineer high-permittivity polymers and ferroelectric liquid crystal phases owing to their high dipole moment.[63,64] Substituting the pendant thiol for a cyano group (LCE-BDMT *vs.* LCE-CN-BM) increases the bulk dielectric constant by ~33%. LCE-EDDET has the highest dielectric constant (ε' = 14.1) and the fastest dipolar relaxation (ε''_{max} at 200 kHz) due to the polar ether linkages that are more flexible than its aromatic/aliphatic counterparts. LCE-EDDET and LCE-CN-BM both exhibit a distinct increase in ε' from 10^2 to 10^{-1}, possibly due to ion poling.[65] Compared to other LCEs, ε' of LCE-EDDET sharply decreases at ~1 Hz (Fig. S1a) and the low-frequency ($\lesssim$1 Hz) dielectric loss factor is an order of magnitude higher. Despite the compelling enhancement to the dielectric constant, ionic polarization is undesirable for DLCEAs due to these associated conductive losses.[40,66] Consistent with these findings, LCE-EDDET had the lowest breakdown voltage.

Dielectric spectroscopy indicates that differences in breakdown strength are not driven by variations in impurity ion content among the as-received comonomers. The increase in low-frequency ε'', which scales with ionic conductivity, is accompanied by a corresponding shift in the M″ peak frequency, suggesting that ionic mobility, rather than ion concentration, dominates the observed behavior (Fig. S1e and S1f). Consistent with this, purification of the monomers prior to polymerization did not alter the properties of the resulting LCEs. Together, these results indicate that changes in dielectric loss and breakdown threshold arise from intrinsic differences in comonomer structure.

Tensile testing and DMA characterize the mechanical behavior of LCEs across a range of temperatures and time scales (Fig. 3). In Fig. 3a, uniaxial tensile moduli parallel and perpendicular to the director are reported. DEAs from monodomain nematic LCEs predominantly deform perpendicular to the director in-plane when stress is applied through-plane. A lower perpendicular modulus predicts greater uniaxial actuation strain, while a higher parallel modulus indicates greater anisotropy and programmability of actuation direction. The onset of the soft elastic plateau and strain hardening for each LCE perpendicular to the alignment director is reported in Fig. 3b. Both are deviations from linear elastic behavior, but the onset of strain hardening for all LCEs is far above the operation regime of DLCEAs manufactured herein. Fig. 3c reports the mechanical loss at ambient conditions, *i.e.* the temperature at which DLCEAs were actuated, and the maximum mechanical loss, which is at the glass transition temperature. The T_g of LCEs is reported in Fig. 3d to conceptualize how proximity to the T_g peak influences mechanics.

In a given formulation, there is wide variation in the moduli measured parallel to the director, particularly for LCE-HDT. We attribute this to sample-to-sample variation in mesogen alignment, arising from the inherent heterogeneity of networks formed *via* thiol-acrylate chain-transfer polymerization. Across all compositions, the small-strain tensile-modulus anisotropy—defined as $Y_{||}/Y_{\perp}$—is $\geq$ 3 for every specimen measured. Models of anisotropic elastomers suggests that deformation is

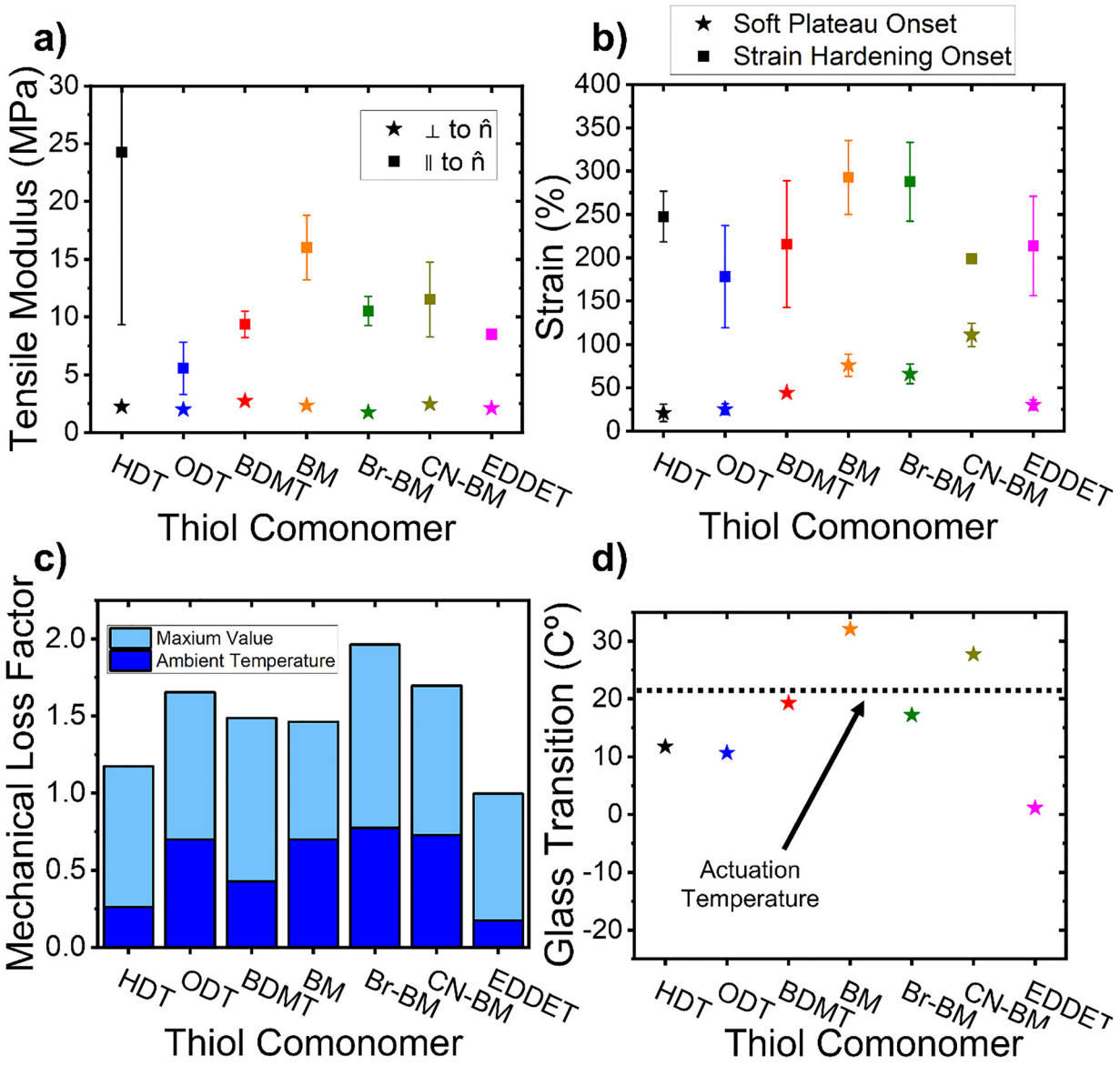

Fig. 3 (a) Tensile modulus of LCEs parallel and perpendicular to director. (b) Onset of the soft elastic plateau and strain hardening for LCEs. (c) Tan(δ)$_{mechanical}$ at 25 °C and at the maximum for each LCE. (d) LCEs' T_g where Tan(δ)$_{mechanical}$ is at a maximum.

predominantly uniaxial at this ratio, and further increases to mechanical anisotropy yield diminishing returns.[43] Although the thiol comonomer affects the stiffness perpendicular to the director, the values for all LCEs fall between 1–3 MPa, the high end of the range suitable for DEAs. Interestingly, the thiol comonomer has a profound effect on the onset of the soft-elastic plateau. Prior reports on LCE-HDT show that once within the soft-elastic plateau, the DEA strain is lower than predicted by the $\varepsilon/Y_{\perp}$ quotient. Differences in the soft-elastic plateau predominantly enable tuning of the thermally driven actuation response; however, only LCE-HDT reached strains high enough to operate under electrostriction within this plateau.

Mechanical loss factor strongly influences the response time and strain magnitude of DLCEAs. Except for LCE-EDDET, all comonomers increase the mechanical loss factor at ambient conditions relative to LCE-HDT. Not only is the absolute magnitude of the tan(δ) peak higher, but T_g is also closer to room temperature. A high degree of network heterogeneity can broaden the temperature window of the tan(δ) peak associated with T_g. Operating closer to T_g increases the mechanical loss factor, reflecting the finite breadth of the glass transition (Fig. S2d). In contrast, LCE-EDDET exhibits both the lowest T_g and the smallest mechanical loss factor. Because T_g lies near or below room temperature, tan(δ) increases with frequency in accordance with time-temperature superposition.[67–69] As a result, mechanical loss is shifted toward shorter time scales. All LCEs examined here follow this expected trend, showing increase in tan(δ) with frequency in the rubbery regime at ambient conditions (Fig. S2c).[47]

All LCEs were actuated for five seconds under a DC electrical bias in 500 V increments across a distance of 30 μm, the total

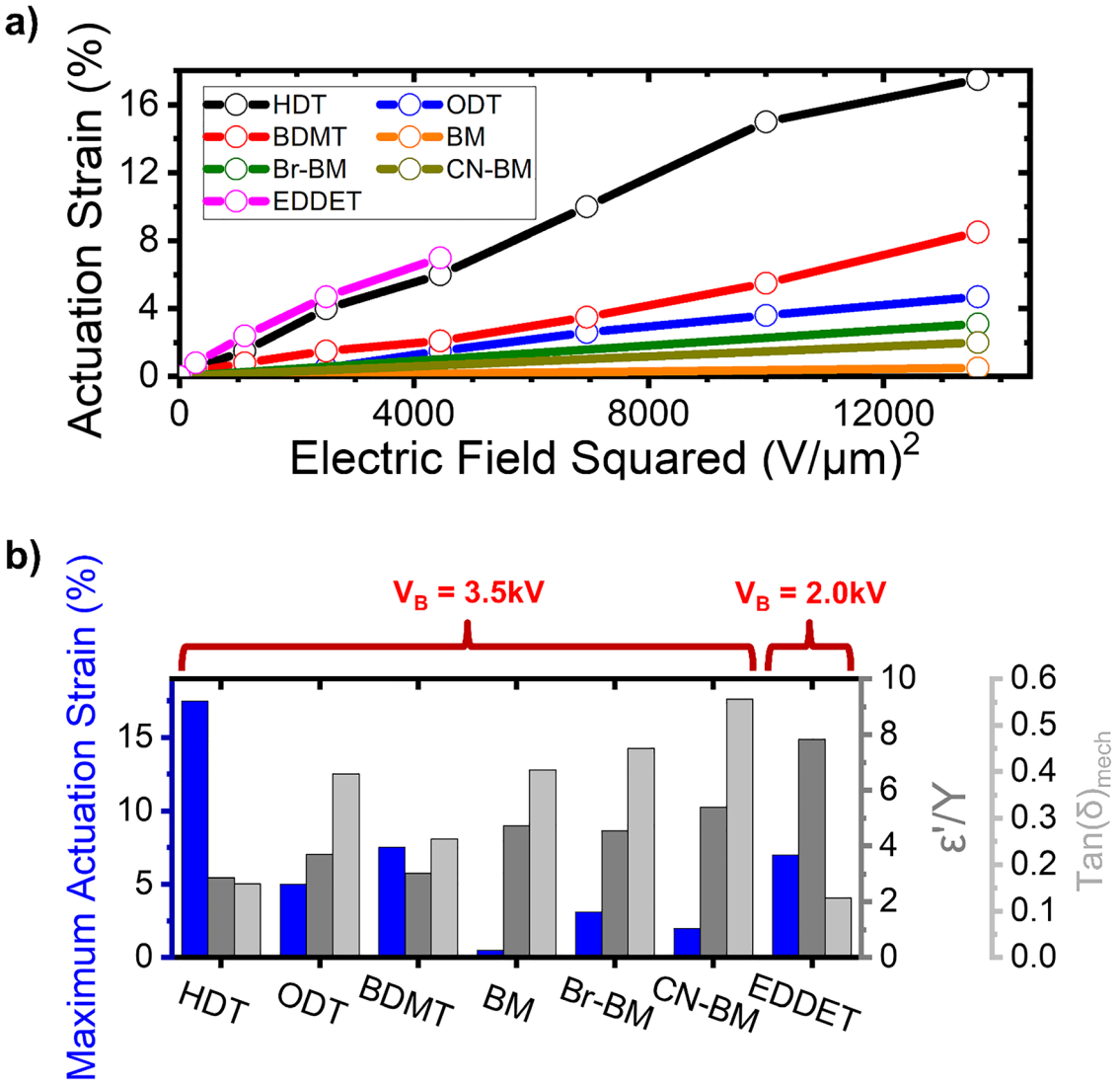

Fig. 4 (a) Strain-voltage response of LCEs under five second DC bias (b) Maximum actuation strain, intrinsic DEA properties quotient ($\varepsilon'/Y_\perp$), and mechanical loss factor at room temperature for all LCEs.

sample thickness. The voltage was raised until the field was high enough to cause dielectric breakdown, rendering the DEAs inoperable. All LCEs failed immediately once the breakdown voltage was applied with no strain response prior, ruling out the electromechanical instability failure mode. Thinner LCEs tend to be easier to manufacture with minimal defects and empirically have a greater dielectric breakdown threshold, so DLCEAs were comprised of two 15 μm films from the same prepolymer mixture laminated together.[47] Fig. 4a shows strain response plotted as a function of electric field squared. The $\varepsilon'/Y_\perp$ quotient predicts DEA strain output at a prescribed electric field provided that strain remains sufficiently small and the system is lossless, *i.e.* the LCE behaves as an ideal capacitor and a hyperelastic solid. The LCEs' modulus perpendicular to the director is chosen for this calculation since strain parallel to the alignment director is negligible. Accordingly, the slope of each DLCEA trace in Fig. 4a is linear and proportional to $\varepsilon'/Y_\perp$ in the ideal case. The $\varepsilon'/Y_\perp$ quotient, the mechanical loss factor, and maximum actuation strain are consolidated in Fig. 4b.

Owing to the low-strain onset of the soft elastic plateau, LCE-HDT is the only formulation to substantially deviate from linearity, particularly at strains $\gtrsim$15%. Counterintuitively, LCE-HDT has the lowest $\varepsilon'/Y_\perp$ quotient but the greatest actuation strain. LCE-EDDET has the steepest strain-voltage curve as predicted by $\varepsilon'/Y_\perp$. However, LCE-EDDET fails at 2 kV, lower than every other LCE tested. This early failure is consistent with elevated dielectric loss and conduction measured at low frequencies. Linearly extrapolating the strain-voltage curve of LCE-EDDET in Fig. 4a suggests the actuation strain would exceed that of LCE-HDT if not for the suppressed breakdown threshold. However, the majority of LCEs have a higher $\varepsilon'/Y_\perp$ quotient than LCE-HDT, have the same breakdown voltage, but still do not reach as high of actuation strains. Disregarding LCE-EDDET because of premature breakdown, the mechanical loss factor is a better predictor of maximum DLCEA strain magnitude. Because the actuation temperature lies within the broad tan(δ) envelope for several formulations, mechanical loss limits

the effective Maxwell stress. Fig. 4b displays that an elevated mechanical loss factor leads to a reduced actuation strain. In this context, mechanical loss arises from the actuation temperature's proximity to T_g. To further probe the role of mechanical loss, we examined both increasing the actuation temperature and decreasing T_g.

DMA indicates LCE-BDMT should reach greater actuation strain at a higher actuation temperature. At a higher temperature, further from T_g, both the tensile modulus and tan(δ) are decreased. Analogously, modifying LCE-BDMT to instead have a lower T_g should suppress mechanical loss and soften the network at ambient conditions. In order to suppress T_g, samples of LCE-BDMT were cured for less time at lower light intensity. Reducing UV dose lowers crosslink density and suppresses T_g without altering chemical composition. Fig. 5a and b compares the mechanical/dielectric behavior of LCE-BDMT polymerized with different UV dosages. Fig. 5c shows the strain-voltage behavior of the identical LCE-BDMT formulations actuated after standard processing, actuated after less UV dosage, and actuated at elevated temperatures.

Lowering the light dosage during curing reduces the crosslink density of samples. This lowers T_g, but increases the height of the tan(δ) peak. Therefore, at room temperature, both light dosages lead to a comparable mechanical loss factor. However, as a consequence of being further above T_g, the less cured sample has a lower storage modulus. The storage modulus provides a small-strain cyclical analog to $Y_\perp$, the tensile modulus relevant to Maxwell stress predictions. The less crosslinked film has an elevated ε'. Reducing crosslinking promotes more ionic mobility and imposes less mechanical constraints on dipole orientation resulting in a more polarizable LCE. This is corroborated by the relaxation peak in the dielectric loss spectra shifting to higher frequencies and increasing in magnitude. Therefore, comparing LCE-BDMT under variable light dosage effectively enables a performance comparison between two systems with identical chemical composition, nearly indistinguishable mechanical loss factors, but different $\varepsilon'/Y_\perp$ quotients. The less cured sample reaches higher strains at a given voltage and has an overall greater maximum actuation strain. This validates the $\varepsilon'/Y_\perp$ quotient as a predictor of DLCEA strain in the absence of other intrinsic material constraints. In fact, the other key difference between the two cure conditions is the difference in dielectric loss. ε' and tan(δ)$_{\text{dielectric}}$ of the less cured system are markedly elevated in the sub-Hz regime. This conductive tail is consistent with the reduced breakdown voltage, 3 kV relative to 3.5 kV, observed under DC actuation. Lower network density promoting increased ionic mobility likely contributes to the reduced breakdown strength.

Alternatively, instead of suppressing T_g to manage mechanical loss at ambient conditions, perhaps actuation strain will be enhanced at elevated temperatures further from the tan(δ) peak at T_g. Fig. 5b shows that the fully cured sample has a lower modulus and mechanical loss factor at elevated temperatures with a local minima of tan(δ) at ~50 °C. When actuated at 50 °C, LCE-BDMT reaches greater actuation strains at a given field, but has substantially reduced breakdown strength, failing at 1.5 kV. Remarkably, this is the same trend seen in the sample where T_g was shifted instead of adjusting the actuation temperature. By actuating above room temperature, the softer and less viscous network more readily deformed at the cost of breakdown threshold.

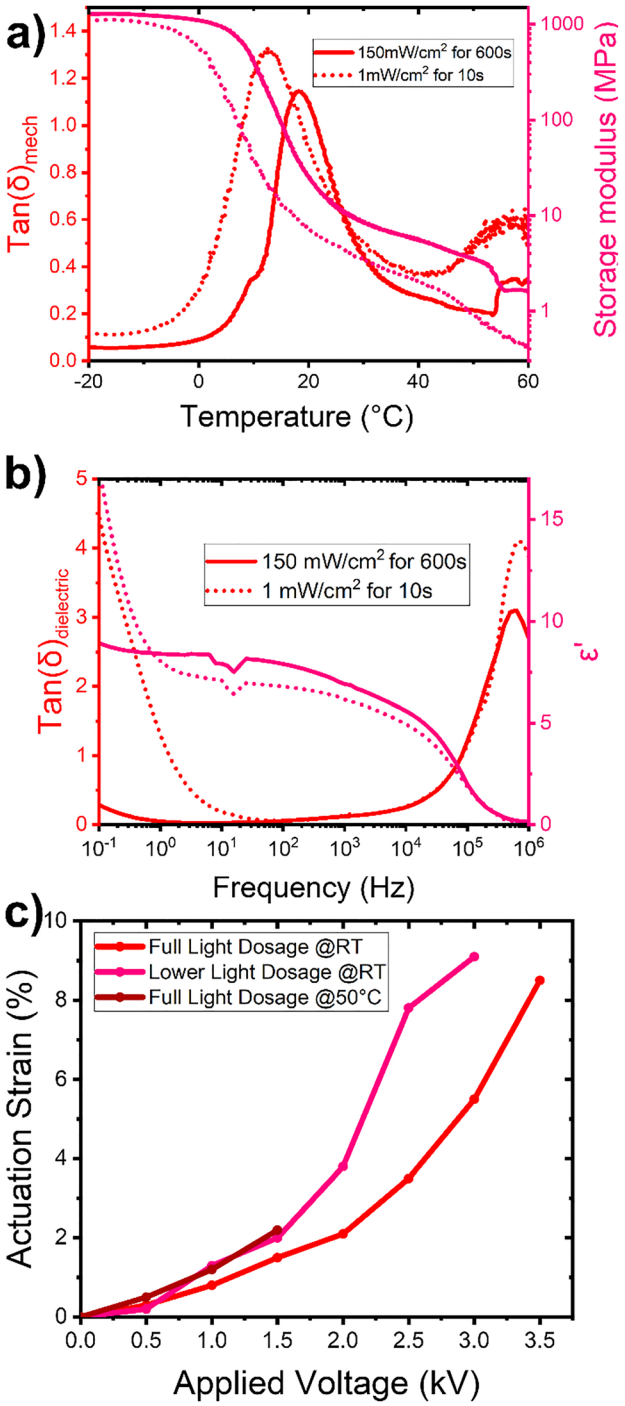

Fig. 5 Comparison of LCE-BDMT cured with different times and light intensities characterized by (a) dynamic mechanical analysis and (b) dielectric spectroscopy. (c) Strain-voltage response under 5s DC bias of fully cured LCE-BDMT at room temperature and 50 °C and partially cured LCE-BDMT at room temperature.

These control experiments highlight one fundamental challenge engineering robust soft materials with high dielectric strength for applications such as DEAs. Simply put, approaches that lower network density, and therefore form soft elastic networks, tend to allow more freedom for ionic motion. In our LCEs, dielectric strength is maximized when the actuation temperature is close to T_g, a trend upheld when shifting the T_g or the actuation temperature. The ionic conductivity of thermoplastics follows an Arrhenius relationship when temperature is below T_g, but then transitions to following a Vogel–Fulcher–Tammann relationship above T_g. In other words, thermoplastics exhibit a marked increase in the temperature dependence of ionic conductivity above T_g as ionic motion becomes coupled to segmental chain motion.[70–72] Although analysis of this phenomena in current LCE[73] or DEA[74] literature is very limited, minimizing the glass transition temperature has long been a dominant strategy for increasing the ionic conductivity of thermoplastic polyelectrolytes.[75–78] The abrupt low-voltage breakdown upon heating our DLCEAs is consistent with a strong dependence of ionic mobility/conductivity as a function of T_g.

LCE-EDDET has a distinctly lower T_g than other LCEs examined. Consequently, LCE-EDDET has the lowest Young's modulus, mechanical loss factor, and breakdown voltage. However, mechanical loss is fundamentally a cyclical measurement, and LCEs are viscoelastic, so the LCEs with a higher mechanical loss factor may reach higher strains over longer time scales. Because short-time actuation tests underpredict strain in mechanically lossy LCEs, long-duration DC bias tests were used to capture the full viscoelastic response. To investigate this, LCEs were held under bias until failure and monitored after the voltage was removed to characterize how much of the strain response is recoverable.

Fig. 6 provides an overview of DLCEAs held under DC bias until failure. A potential of 2.5 kV was selected to balance strain output with device lifetime. LCE-EDDET is omitted as it is not stable under field for long time scales. Samples were stable under field for approximately five minutes, aside from a few champion devices with longer lifetimes. Although a full constitutive description would have immense utility, such models that incorporate dynamic electromechanics in anisotropic materials remain difficult to fit to real data sets. Prony series are a well-established numerical method for quantifying experimentally realized viscoelastic effects in DEAs.[79–82] Our strain evolution is fit to a KWW stretched exponential which is mathematically equivalent to an infinite Prony series. This approach utilizes three fitted parameters: strain after infinite time has elapsed, the time constant by which strain grows/decays, and a stretching factor to describe the breadth of time scale distribution. Fig. 6a shows the experimental and theoretical strain response of DLCEAs under an applied field alongside the actuation time constant and theoretical maximum achievable strain. Fig. 6b shows recovery after the removal of the field as well as the recovery time constant and fraction of recoverable strain.

The model fits well with the measured DLCEA behavior which is particularly evident in LCE-Br-BM which was stable under field for a full hour across multiple samples. Choice of

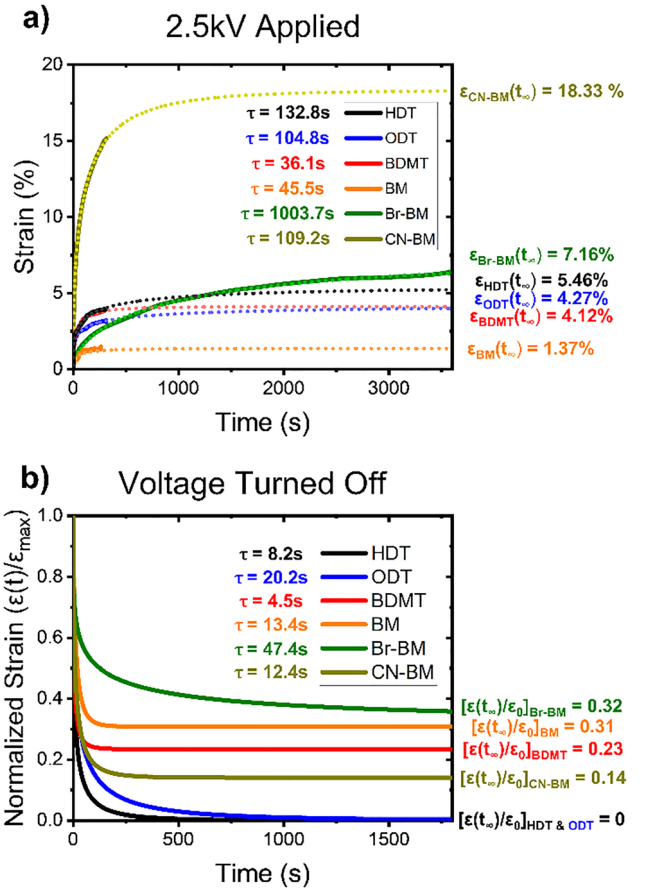

Fig. 6 (a) Strain response over time of DLCEAs under 2.5 kV DC bias shown experimentally (solid) and theoretically (dotted) (b) relaxation response of DLCEA after removal of 2.5 kV bias normalized to maximum actuation strain.

comonomer strongly influences the time-dependence of the actuation response: LCEs with lower mechanical loss factors deform more in the first few seconds (Fig. S2a). LCE-HDT has the lowest tan(δ) across the full frequency range measured and therefore reaches the highest actuation strain in a few seconds. LCE-CN-BM has a high dielectric constant and high mechanical loss factor, so the immediate actuation reduced is shorter, but eventually reaches a maximum value of 15.3% strain and is projected to reach 18.3% if field stability was not a limitation. Because tan(δ) is simply the fraction of viscous to elastic deformation, this parameter is insufficient to predict the rate and recoverability of deformation. Despite highly variable tan(δ) values, only LCE-HDT and LCE-ODT, were able to fully return to original sample dimensions. Compared to LCE-ODT, LCE-BM has a similar tan(δ) and LCE-BDMT a notably lower tan(δ), yet 31% and 23% of LCE-BM and LCE-BDMT strain was permanent, respectively. LCE-Br-BM has a comparable tan(δ) to LCE-CN-BM, but the time scale of actuation is an order of magnitude higher and 32% of deformation was permanent compared to the 14% of the LCE-CN-BM counterpart.

Another key result is that relaxation times were consistently faster than the actuation response, as evidenced by the data in

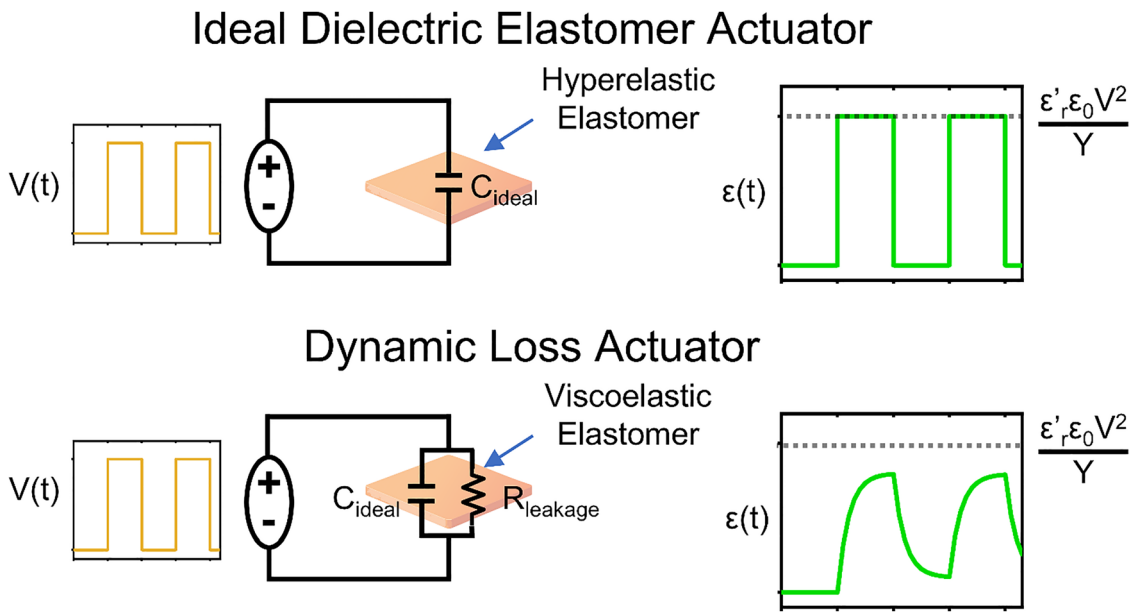

Fig. 7 Schematic showing how real DEAs deviate from directly scaling with Maxwell stress and Young's modulus due to dynamic losses: leakage currents, viscous dissipation, and delayed electromechanical coupling.

Fig. 6. Thus, there are time-dependent electromechanical effects that only occur under field. This indicates electrical effects slow actuation in addition to the innate viscosity of LCEs. The slowed actuation response could be intrinsic to the time-dependence of the polarization of LCE under field, but this is unlikely since the ε' plateau extends to several kHz across all LCEs. We speculate that the electrode/wiring setup held consistent across all LCEs was responsible for slowing charge accumulation processes, but further study is needed. Nonetheless, the consistently faster relaxation relative to actuation suggests that dissipation under field, not post-field viscoelastic recovery, governs DLCEA stroke.

These long-time studies reveal that both LCE-Br-BM and LCE-CN-BM reach higher actuation strains than the prior formulation (LCE-HDT). LCE-Br-BM and LCE-CN-BM have the highest mechanical loss factors out of all LCEs reported herein. Given infinite time and no limitations from breakdown stability, LCE-Br-BM and LCE-CN-BM are predicted to reach 7.16% and 18.33% strain at 2.5 kV, respectively. LCE-Br-BM undergoes slow and highly plastic deformation. Owing to the relaxation time constant of 47.4 seconds, several minutes are required to even recover half of the total actuation strain and only 68% of strain is theoretically recoverable. By contrast, 86% of the overall strain output is reversible in LCE-CN-BM; performance rivaled only by the aliphatic comonomers (HDT and ODT). Both LCE-Br-BM and LCE-CN-BM exhibit high permittivity and high mechanical loss, leading to slow but large long-duration strains under sustained DC bias. In other words, increasing the dielectric constant does improve actuation strain, but dissipative mechanical processes slow and supress the actuation response. This informs future design, as the viscoelasticity of LCEs produced *via* chain transfer chemistry limits the DEA response time even with elevated Maxwell stress output.

The difference between the real DLCEAs tested herein and those posited by the approximation in eqn (1) are visualized and reviewed in Fig. 7. Increasing the dielectric constant does increase Maxwell stress, but other intrinsic properties respond to compositional changes. Namely, energy that would otherwise manifest as actuation strain is lost to leakage current and viscous dissipation. These properties innate to real viscoelastic LCEs ensure time-dependent electromechanical coupling.

Conclusions

A series of aligned LCEs are implemented as the dielectric layer in DEA devices. We demonstrate that the dielectric constant can be bolstered, and the $\varepsilon'/Y_\perp$ quotient can be modulated, by choice of comonomer. Actuation testing reveals that the $\varepsilon'/Y_\perp$ quotient is a poor predictor of the strain-voltage relation in mechanically lossy LCEs. DMA reveals that elevated mechanical loss can arise from the glass transition peak overlapping with the actuation temperature. However, DS and actuation testing reveal that furthering the distance between T_g and the operation temperature increases dielectric losses and lowers the breakdown voltage. In LCEs made with chain transfer chemistry, tuning the broad glass transition peak either direction results in increased mechanical or electronic energy dissipation.

Mechanically lossy LCE with high dielectric constants can reach higher actuation strain, but only over the course of many minutes which may prove desirable for preventing pull-in failure/electromechanical instability at actuation frequencies. Therefore, DLCEAs may also find utility in soft robotics applications where directional response and electronic control are prioritized over response time. DLCEAs are therefore well-suited for soft robotic applications where directional response

and electronic control are prioritized over response time. LCE-HDT is best suited for short-term, muscle-like actuation due to its rapid response and full recovery. In contrast, LCE-CN-BM is more effective for long-term, quasi-static actuation, offering higher strain per voltage with moderate response and recovery. Across all systems, the retained modulus anisotropy enables strong directional programmability *via* electrostriction. Future LCE chemistries may avoid dissipative mechanisms through alternative molecular design tactics. Classical DEAs fail from all variety of phenomena such as electromechanical instability or mechanical rupture, but the only failure mechanism of DLCEAs reported to date is dielectric breakdown. This work highlights the need to improve the dielectric breakdown threshold of LCEs and the pragmatic challenges in doing so. Improving the breakdown strength and/or response time of DLCEAs is a key step to their realization as a platform for programmable soft actuation.

Author contributions

J.M.S., H.E.F, and T.J.W. conceived the study. T.J.W. led the project. J.M.S. and T.J.W. wrote the manuscript with input from all authors. J.M.S. fabricated and characterized the DLCEAs with assistance from H.E.F. and A.H. All authors have given approval to the final version of the manuscript.

Conflicts of interest

There are no conflicts to declare.

Data availability

The data supporting this article are included within the article and its supplementary information (SI). Supplementary information: FTIR. Additional mechanical and electronic characterization of LCEs. Parameters for theoretical fit of DLCEA actuation and relaxation. See DOI: https://doi.org/10.1039/d6tc00536e.

Additional data that support the findings of this study are available from the corresponding author upon reasonable request.

Acknowledgements

The authors are grateful for financial support from the University of Colorado and the Air Force Research Laboratory.

References

1 J. M. McCracken, B. R. Donovan and T. J. White, *Adv. Mater.*, 2020, **32**, e1906564.
2 C. Ohm, M. Brehmer and R. Zentel, *Adv. Mater.*, 2010, **22**, 3366–3387.
3 Y. Yu and T. Ikeda, *Angew. Chem., Int. Ed.*, 2006, 45, 5416–5418.
4 J. Hu, M. Yu, M. Wang, K. L. Choy and H. Yu, *ACS Appl. Mater. Interfaces*, 2022, **14**, 12951–12963.
5 E. B. Priestley, P. J. Wojtowicz and P. Sheng, *Introduction to Liquid Crystals*, Springer, New York, NY, 1st edn, 1975.
6 J. W. Goodby, in *Handbook of Liquid Crystals: Fundamentals of Liquid Crystals*, ed. J. W. Goodby, P. J. Collings, T. Kato, C. Tschierske, H. F. Gleeson, P. Raynes and V. Vill, Wiley-VCH, Weinheim, 2nd edn, 2014, vol. 1, ch. 3, pp. 59–76.
7 D. Thomas, M. Cardarelli, A. Sánchez-Ferrer, B. L. Mbanga, T. J. Atherton and P. Cebe, *Liq. Cryst.*, 2015, **43**, 112–123.
8 J. M. McCracken, B. R. Donovan, K. M. Lynch and T. J. White, *Adv. Funct. Mater.*, 2021, **31**, 2100564.
9 K. L. Lewis, J. D. Hoang, M. F. Toney and T. J. White, *Chem. Mater.*, 2024, **37**(1), 175–188.
10 T. J. White and D. J. Broer, *Nat. Mater.*, 2015, **14**, 1087–1098.
11 C. Zhang, G. Chen, K. Zhang, B. Jin, Q. Zhao and T. Xie, *Adv. Mater.*, 2024, e2313078, DOI: 10.1002/adma.202313078.
12 D. Duffy, J. M. McCracken, T. S. Hebner, T. J. White and J. S. Biggins, *Phys. Rev. Lett.*, 2023, **131**, 148202.
13 Y. Wang, J. Sun, W. Liao and Z. Yang, *Adv. Mater.*, 2022, **34**, e2107840.
14 J. Sun, Y. Wang, W. Liao and Z. Yang, *Small*, 2021, **17**, e2103700.
15 V. Maurin, Y. Chang, Q. Ze, S. Leanza, J. Wang and R. R. Zhao, *Adv. Mater.*, 2024, **36**, e2302765.
16 R. Kornbluh, R. Peirine, J. Joseph, R. Heydt, Q. Pei and S. Chiba, *Smart Structures and Materials 1999: Electroactive Polymer Actuators and Devices*, SPIE, Bellingham, WA, 1999.
17 R. E. Pelrine, R. D. Kornbluh and J. P. Joseph, *Sens. Actuators, A*, 1998, **64**, 77–85.
18 R. Kornbluh, R. Peirine, Q. Pei, S. Oh and J. Joseph, *Smart Structures and Materials 2000: Electroactive Polymer Actuators and Devices*, SPIE, Bellingham, WA, 2000.
19 A. O'Halloran, F. O'malley and P. McHugh, *J. Appl. Phys.*, 2008, **104**, 071101.
20 Y. Wang, X. Ma, Y. Jiang, W. Zang, P. Cao, M. Tian, N. Ning and L. Zhang, *Resour. Chem. Mater.*, 2022, **1**, 308–324.
21 E. Hajiesmaili and D. R. Clarke, *J. Appl. Phys.*, 2021, **129**, 151102.
22 F. Carpi, D. De Rossi, R. Kornbluh, R. E. Pelrine and P. Sommer-Larsen, *Dielectric elastomers as electromechanical transducers: Fundamentals, materials, devices, models and applications of an emerging electroactive polymer technology*, Elsevier, 2011.
23 L. Zhang, S. Qu and X. Du, *Adv. Intell. Syst.*, 2021, **3**, 2100173.
24 L. Yang, H. Wang, D. Zhang, Y. Yang and D. Leng, *Chem. Eng. J.*, 2024, 151402.
25 Y. Chen, H. Zhao, J. Mao, P. Chirarattananon, E. F. Helbling, N. P. Hyun, D. R. Clarke and R. J. Wood, *Nature*, 2019, **575**, 324–329.
26 R. Pelrine, R. Kornbluh, Q. Pei and J. Joseph, *Science*, 2000, **287**, 836–839.
27 A. Wiranata, M. Kanno, N. Chiya, H. Okabe, T. Horii, T. Fujie, N. Hosoya and S. Maeda, *Appl. Phys. Express*, 2021, **15**, 011002.
28 C. Tang, B. Du, S. Jiang, Z. Wang, X.-J. Liu and H. Zhao, *Adv. Intell. Syst.*, 2024, **6**, 2300047.

29 J.-H. Youn, S. M. Jeong, G. Hwang, H. Kim, K. Hyeon, J. Park and K.-U. Kyung, *Appl. Sci.*, 2020, **10**(2), 640.
30 T. Vu-Cong, C. Jean-Mistral and A. Sylvestre, *Smart Mater. Struct.*, 2012, **21**(10), 105036.
31 S. Michel, X. Q. Zhang, M. Wissler, C. Löwe and G. Kovacs, *Polym. Int.*, 2009, **59**, 391–399.
32 F. Schneider, T. Fellner, J. Wilde and U. Wallrabe, *J. Micromech. Microeng.*, 2008, **18**, 065008.
33 I. D. Johnston, D. K. McCluskey, C. K. Tan and M. C. Tracey, *J. Micromech. Microeng.*, 2014, **24**, 035017.
34 S. Li, J. Zhang, J. He, W. Liu, Y. Wang, Z. Huang, H. Pang and Y. Chen, *Adv. Sci.*, 2023, **10**, 2304506.
35 E. Taine, T. Andritsch, I. A. Saeedi and P. H. Morshuis, *Energies*, 2023, **16**, 7424.
36 Y. Sheima, J. von Szczepanski, P. M. Danner, T. Künniger, A. Remhof, H. Frauenrath and D. M. Opris, *ACS Appl. Mater. Interfaces*, 2022, **14**, 40257–40265.
37 J. Huang, X. Zhang, R. Liu, Y. Ding and D. Guo, *Nat. Commun.*, 2023, **14**, 1483.
38 H. Sato and T. Hirai, 2013.
39 Z. Zhang, A. Wang, T. Chen, T. Wang and P. Li, *Macromol. Chem. Phys.*, 2025, **226**, 2400447.
40 P. Brochu and Q. Pei, *Macromol. Rapid Commun.*, 2010, **31**, 10–36.
41 C. Löwe, X. Zhang and G. Kovacs, *Adv. Eng. Mater.*, 2005, **7**, 361–367.
42 K. Shimizu, T. Nagai and J. Shintake, *Polymers*, 2021, **13**(24), 4310.
43 J. He, Z. Chen, Y. Xiao, X. Cao, J. Mao, J. Zhao, X. Gao, T. Li and Y. Luo, *ACS Mater. Lett.*, 2022, **4**, 472–479.
44 Z. S. Davidson, 2019.
45 H. E. Fowler, H. M. Pearl and T. J. White, *Adv. Mater. Technol.*, 2024, **9**(9), 2301970.
46 R. Annapooranan, Y. Wang and S. Cai, *Adv. Mater. Technol.*, 2023, **8**(9), 2201969.
47 H. E. Fowler, P. Rothemund, C. Keplinger and T. J. White, *Adv. Mater.*, 2021, **33**, e2103806.
48 H. Zhao, Z. Chen, J. Li, Y. Luo, Z. Peng, G. Mao, R. Xiao and J. Mao, *Sci. Adv.*, 2025, **11**, eaeb2289.
49 F. B. Albuquerque and H. Shea, *Smart Mater. Struct.*, 2020, **29**(10), 105024.
50 Z. Wang, B. He, Y. Zhou, R. Shen and G. Li, *Int. J. Mech. Sci.*, 2020, **185**, 105879.
51 A. Tröls, A. Kogler, R. Baumgartner, R. Kaltseis, C. Keplinger, R. Schwödiauer, I. Graz and S. Bauer, *Smart Mater. Struct.*, 2013, **22**, 104012.
52 Y. Qiu, E. Zhang, R. Plamthottam and Q. Pei, *Acc. Chem. Res.*, 2019, **52**, 316–325.
53 M. W. M. Tan, G. Thangavel and P. S. Lee, *NPG Asia Mater.*, 2019, **11**, 62.
54 X. Zhao, S. J. A. Koh and Z. Suo, *Int. J. Appl. Mech. Eng.*, 2011, **3**, 203–217.
55 A. Kumar, A. Khurana, A. K. Sharma and M. Joglekar, *J. Braz. Soc. Mech. Sci. Eng.*, 2022, **44**, 348.
56 L. Zhang, X. Shi, G. Gu, J. Zou and J. Liu, *Mech. Syst. Signal Process.*, 2025, **241**, 113405.
57 L. T. Creagh and A. R. Kmetz, *Mol. Cryst. Liq. Cryst.*, 1973, **24**, 59–68.
58 K. M. Herbert, H. E. Fowler, J. M. McCracken, K. R. Schlafmann, J. A. Koch and T. J. White, *Nat. Rev. Mater.*, 2021, **7**, 23–38.
59 M. Warner, P. Bladon and E. Terentjev, *J. Phys. II*, 1994, **4**, 93–102.
60 K. K. Chi, 2004.
61 L. Zhu, *J. Phys. Chem. Lett.*, 2014, **5**, 3677–3687.
62 T. S. Hebner, H. E. Fowler, K. M. Herbert, N. P. Skillin, C. N. Bowman and T. J. White, *Macromolecules*, 2021, **54**, 11074–11082.
63 S. J. Dünki, M. Tress, F. Kremer, S. Y. Ko, F. A. Nüesch, C.-D. Varganici, C. Racles and D. M. Opris, *RSC Adv.*, 2015, **5**, 50054–50062.
64 M. Hird, *Liq. Cryst.*, 2011, **38**, 1467–1493.
65 P. Simon and Y. Gogotsi, *Nat. Mater.*, 2008, **7**, 845–854.
66 F.-C. Chiu, *Adv. Mater. Sci. Eng.*, 2014, **2014**, 578168.
67 R. Annapooranan, S. Suresh Jeyakumar, R. J. Chambers, R. Long and S. Cai, *Adv. Funct. Mater.*, 2024, **34**, 2309123.
68 H. Fang, F. Zhang, Y. Zhao, X. Gao, W. Zhou, G. Qi, Y. Ding and H. H. Winter, *Macromolecules*, 2023, **56**, 7808–7817.
69 A. Hotta and E. Terentjev, *J. Phys.: Condens. Matter*, 2001, **13**, 11453–11464.
70 V. Popova and N. Surovtsev, *Phys. Rev. E:Stat., Nonlinear, Soft Matter Phys.*, 2014, **90**, 032308.
71 A. Roggero, N. Caussé, N. Pébère and E. Dantras, *Polymer*, 2022, **241**, 124542.
72 M. Petrowsky and R. Frech, *J. Phys. Chem. B*, 2009, **113**, 5996–6000.
73 T. Raistrick, M. Reynolds, H. F. Gleeson and J. Mattsson, *Molecules*, 2021, **26**, 7313.
74 C. Zeytun Karaman, T. Raman Venkatesan, F. A. Nüesch and D. M. Opris, *ACS Appl. Mater. Interfaces*, 2025, **17**(26), 38504–38514.
75 C. A. Vincent, *Electrochim. Acta*, 1995, **40**, 2035–2040.
76 J. Imbrogno, K. Maruyama, F. Rivers, J. R. Baltzegar, Z. Zhang, P. W. Meyer, V. Ganesan, S. Aoshima and N. A. Lynd, *ACS Macro Lett.*, 2021, **10**, 1002–1007.
77 W. C. Chen, H. H. Chen, T. C. Wen, M. Digar and A. Gopalan, *J. Appl. Polym. Sci.*, 2004, **91**, 1154–1167.
78 Y. Wang, A. L. Agapov, F. Fan, K. Hong, X. Yu, J. Mays and A. P. Sokolov, *Phys. Rev. Lett.*, 2012, **108**, 088303.
79 R. S. Lakes, *Viscoelastic solids (1998)*, CRC press, 2017.
80 R. K. June, J. P. Cunningham and D. P. Fyhrie, *Biomed. Eng. Res.*, 2013, **2**, 153.
81 M. Wissler and E. Mazza, *Sens. Actuators, A*, 2007, **134**, 494–504.
82 J. Zhang, J. Ru, H. Chen, D. Li and J. Lu, *Appl. Phys. Lett.*, 2017, **110**(4), 044104.